A Novel Heatsink Attached mm-Wave Active Patch Antenna With Adjustable Frequency and Cooling

Celik, Feza; Aslan, Yanki

DOI
10.23919/EuCAP57121.2023.10133134

Publication date
2023

Document Version
Final published version

Published in
Proceedings of the 2023 17th European Conference on Antennas and Propagation (EuCAP)

A Novel Heatsink Attached mm-Wave Active Patch Antenna With Adjustable Frequency and Cooling

Feza Turgay Celik*, Yanki Aslan†
Microwave Sensing, Signals and Systems Group, Department of Microelectronics,
Faculty of Electrical Engineering, Mathematics, and Computer Science,
Delft University of Technology, Delft, The Netherlands
{*F.T.Celik, †Y.Aslan}@tudelft.nl

***Abstract*—In this study, the thermal management problem of the modern communication systems with small array sizes is addressed. A novel dual-functional active antenna design strategy is introduced for adjustable frequency of operation and cooling extension at millimeter-wave bands. The concept is based on placing different types of heatsinks on the same patch antenna. The electromagnetic and thermal behavior of the proposed heatsink structures are presented via simulations. Reconfigurable operation at 24, 26, and 28 GHz frequencies with 23 to 28 degrees of extra cooling in the chip as compared to the conventional patch is achieved.**

***Index Terms*—active integrated antenna, cooling, frequency reconfiguration, heatsink antenna, millimeter-wave communication.**

I. Introduction

Future telecommunication technologies require more speed and capacity. The ambitious data rate can be supplied by the Massive Multiple-Input Multiple-Output (M-MIMO) technology in the millimeter-wave (mm-wave) frequencies covering 24 GHz (low end), 26 GHz (n258), and 28 GHz (n257) bands [1]. Due to the short wavelengths at these frequencies. the active array structures become physically small, which leads to very high heat densities [2] and significant cooling problems for the radio-frequency (RF) beamformer chips [3].

The conventional electronics thermal management techniques employing heatsinks, heatpipes, fans or liquid channels focus on cooling the array system only from the chip side [4]. This results in impractical, bulky and energy-inefficient products [5], [6]. The emerging concept of heatsink antenna, which utilizes the antenna itself as a heat dissipator on the opposite side of the board, is promising to alleviate such issues by providing additional cooling paths [7].

About a decade ago, microstrip antennas with heatsinks on top were studied in the sub-6 GHz bands [8], [9]. These studies focused only on the electromagnetic effects of the rectangular fins and did not include thermal considerations. Recently, mm-wave slot antennas fed by substrate integrated waveguides (SIWs) and incorporating rectangular fins were proposed [10], [11]. As the SIW helps the antenna system convey the excess heat from the chip to the antenna side easily, cooling extension through the fin structures was observed. However, these studies did not use a proper thermal model for the chips for reliable temperature simulations. Besides, they suffer from the difficulties and costs of SIW design, and the negative effects of the fin structure in the radiation pattern.

In this paper, we propose a unique reconfigurable frequency dual-functional antenna concept with interchangeable pin fin heatsink structures on basic coaxial-fed microstrip patch. Heatsink structures are employed to increase the convection surface. The electromagnetic and thermal model of a shorted patch and the heatsink antenna are described in Section II. The impact of the heatsink on impedance matching is investigated in Section III via parametric studies. Three novel heatsink antennas for adjustable frequency are introduced in Section IV with their numerical results on cooling and electromagnetic performance. Conclusions are drawn in the Section V.

II. Antenna Modeling

A. Shorted Patch Antenna - Electromagnetic Model

As the heatsink structure on top of the patch needs to be changed, the antenna element should be simple to prevent mounting errors. Therefore, a standard rectangular patch (fed by a coaxial probe for simulation purposes) is preferred. To have a large heat exchange surface, the ratio of the length and width of the antenna is selected as 1.11. Rogers 5880 with 0.252 mm thickness is used due to its low dielectric loss ($\gamma = 0.0009$) and low permittivity ($\epsilon_r = 2.2$). As the Rogers 5880 has very low thermal conductivity, the excess heat accumulated in the chip beneath the dielectric cannot be conducted to the patch. To create a conductive path from the chip to the patch, a shorted patch antenna type is developed by inserting five conducting vias from the central line of the

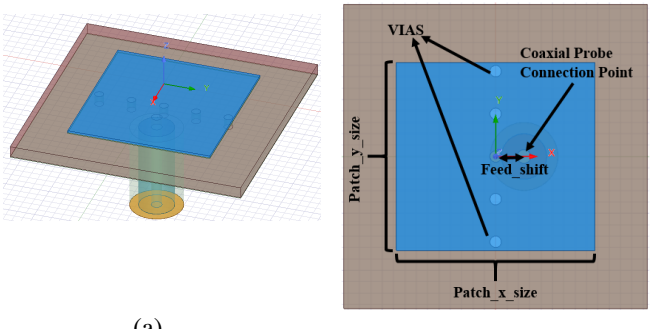

(a) (b)

Fig. 1. The shorted patch antenna: (a) isometric view, (b) side view. (Patch_x_size = 3.37 mm, Patch_y_size = 3.3 mm, Feed_shift = 0.5 mm)

radiating patch to the ground plate and to the face of the chip (see Fig. 1). The via radii are selected as 0.2 mm.

B. Heatsink Antenna - Electromagnetic Model

The fined heatsink made out of copper is placed on top of the patch antenna given in Fig. 1 with no change in the patch size, feed position and coaxial probe. To have a more realistic scenario a thermal paste is used in between. The thermal paste is assumed to be dielectric-based with $\epsilon_r = 4.4$ and thickness of 0.05 mm. The electromagnetic modeling and simulations of the shorted patch and heatsink antennas were performed in ANSYS HFSS.

C. Heatsink Antenna - Thermal Model

Since the dual-functionality of the antenna is aimed to be shown, the designs are also simulated in the thermal simulator ANSYS ICEPAK. Following the literature [4], [6], the chips are modeled with the two resistor model [12] as explained in Fig. 2. The two resistor model defines the junction as the main heat source and then creates two heat conduction paths to the case and the board side of the chip. The characteristics of a particular chip are defined by the values of the junction power level, and the thermal resistances between junction to case (Rjc) and junction to board (Rjb). Thermal simulations are realized under forced air condition. The air is assumed to flow in lateral direction with 2m/s initial velocity. Fig. 2a provides the thermal network. Fig. 2b lists the model parameter settings [6] of the chip whose dimensions are 4.3 x 3.5 x 0.5 mm. The temperature distribution and air velocity vectors simulated from ICEPAK are shown in Fig. 2c and Fig. 2d, respectively. For better visualization, the side view of a complete thermal modeling for a heatsink antenna is given in Fig. 3.

III. Parametric Analysis on Heatsink Structures

Here, the thermal and electromagnetic effects of the fin parameters are discussed. The focus of the simulations is on the nine elements of cylindrical fin structure whose isometric illustration and dimensions can be seen in Fig. 4. To understand the effect of fin elements parametric studies are studied on fin base thickness (h_b), fin height (h_c for central and h_s for side), the separation between fins (d), and fin radius (r).

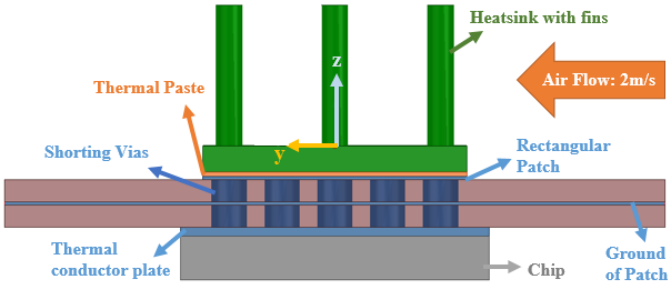

Fig. 3. Thermal simulation model for the heatsink antennas with layer visualization in transparent side view.

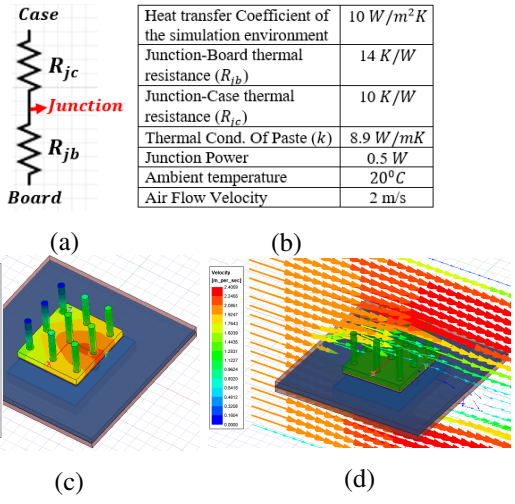

Heat transfer Coefficient of the simulation environment	$10\ W/m^2K$
Junction-Board thermal resistance (R_{jb})	$14\ K/W$
Junction-Case thermal resistance (R_{jc})	$10\ K/W$
Thermal Cond. Of Paste (k)	$8.9\ W/mK$
Junction Power	$0.5\ W$
Ambient temperature	20^0C
Air Flow Velocity	2 m/s

Fig. 2. Thermal simulation model: (a) two resistor model, (b) thermal parameters, (c) a sample heat distribution on fins and (d) air velocity vectors.

A. Fin Basis

Fin basis is a bulky metallic structure hosting cylindrical fins that are thermally connected to the patch antenna with thermal paste. As the thermal paste is very thin as compared to the wavelength, the surface currents excited on the patch structure are induced on the fin base. Therefore, the radiation of the fin base is the same as the patch antenna. Although variation in fin basis preserve radiation pattern of the structure, it changes the thermal performance of the antenna dramatically. Since a thicker fin base structure behaves like huge heat storage, it can draw more heat from the chip and spread to the air with the help of fins and forced air. However, there is a limit on how much heat can be drawn by the heatsink and that limit is defined by the shorting vias and the thermal conductor plate of the chip structure (see Fig. 3). In Fig. 5 the $|S_{11}|$ parameters under different fin base height (h_b) values can be seen.

It can be understood from this figure that the resonance frequency of the antenna shifts to the lower bands as the fin base gets thicker, and bandwidth decreases. The change in the resonance frequency is related to the induced currents on the fin base structure. The thicker it gets, the surface currents

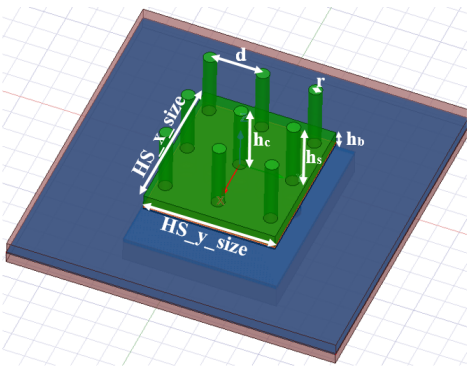

Fig. 4. Isometric view of the heatsink model and its dimensions. (HS_x_size = 3.33 mm, HS_y_size = 3 mm)

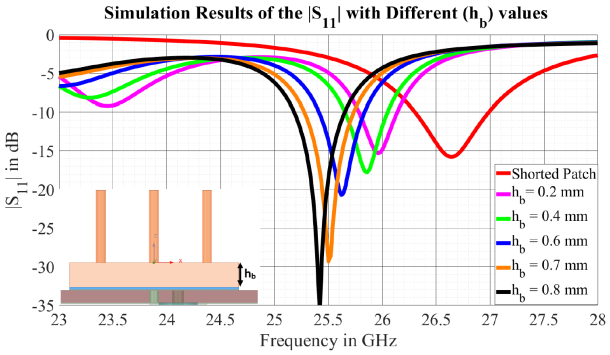

Fig. 5. Frequency dependence of the reflection coefficient for different fin base thicknesses(h_b). ($h_c = h_s = 1.5, d = 1.2, r = 1.5mm$)

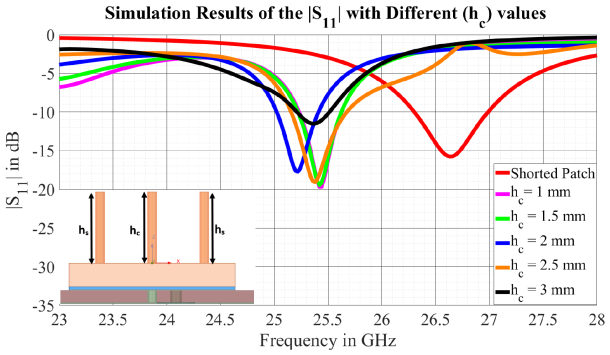

Fig. 7. Frequency dependence of the reflection coefficient for different central fin heights(h_c). ($h_s = 1.5, h_b = 0.3d = 1.2, r = 1.5mm$)

need to travel greater distances and the resonance frequency of the structure decreases. In the final designs, the heatsink thickness is selected as 0.3 mm as the thermal performance of the heatsink is limited by the shorting vias there is no meaning in using a thicker heatsink basis as it will deteriorate the radiation pattern.

B. Common Fin Height

In addition to the heatsink base, the fin heights also have an important effect on both the electromagnetic and thermal performance of the antenna array. Frequency dependence of the reflection coefficient for different fin base thicknesses of the antenna with different h_s = h_c heights is shown in Fig. 6.

In this figure, the height of each fin is kept equal to each other. The decrease in the resonance point with increasing fin height can easily be observed. The antenna having h_s = 0.5 mm has a higher resonance frequency at the desired mode than the h_s = 2.3 mm one. This result was quite expected because it can be understood that the increase in the fin height will extend the surface current path and so resonate in the lower frequency. However, this behavior also has some restrictions. The fin height determines the dominant operation principle of the antenna. At 28 GHz the λ/4 value is 2.6 mm, so the fins having a height of more than 2.3 mm start to create a monopole structure. The design that uses fins more than 2.3 mm would not behave as a single patch antenna but it acts as a patch

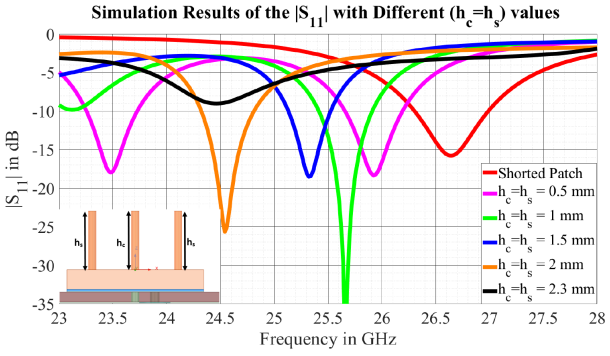

Fig. 6. Frequency dependence of the reflection coefficient for different fin heights(h_c = h_s).($h_b = 0.3, d = 1.2, r = 1.5mm$)

antenna and six monopole structures at the radiating edges of the antenna. This creates very different and non-practical radiation patterns; therefore, we avoided monopole excitation in the interest region by selecting h_s = 1.5 mm.

C. Central Fin Height

Even though the fin structures at the antenna edges have size limitations, this limitation is not the same for the fins in the middle side of the antenna. The reflection coefficient simulations of different h_c values under the same h_s condition can be seen in Fig. 7.

In this parametric sweep, the fin heights at the radiating sides of the patch (h_s) are kept constant, only fins at the central lines (h_c) are changed. The central fin size does not have an effect on the resonance frequency. These fin structures coincide with the shorting vias. Therefore, they are located at the potential zero point of the antenna. This placement makes the radiation pattern of the antenna immune to the central fin height changes. Though it seems that we have full freedom to change the height of the central fin, it is restricted by the reflection coefficient value. When the h_c increases the additional impedance added to the antenna changes. After h_c = 2.5 mm, the additional impedance coming from central fins distorts the antenna input impedance and yields excess reflections as seen in Fig. 7. Due to impedance restrictions, the h_c value of this design is selected as 1.7 mm.

D. Distance Between Fins

The distance between fins affects the reflection coefficient and radiation pattern. The reflection coefficient values in different fin separation (d) values can be seen in Fig. 8.

Distance between fins determines the excess path that is introduced to the antenna and so it changes the resonance frequency. The resonance frequency of the antenna decreases with the fin separation (Fig. 8). Although the reflection coefficient of the antenna stays in an acceptable range, the radiation pattern of the antenna is affected severely by the fin location. When the fins are located at the radiating edges (d = 1.2 mm), radiation from vertical fins becomes more dominant. This effect distorts the polarization of the antenna. The regular patch antenna in our case, has polarization on the E-plane

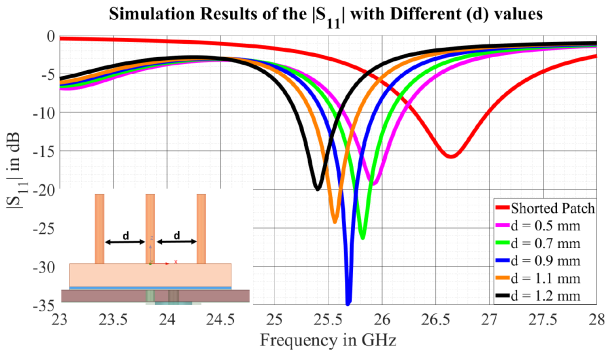

Fig. 8. Frequency dependence of the reflection coefficient for different fin separations(d). ($h_c = h_s = 1.7, h_b = 0.3, r = 1.5mm$)

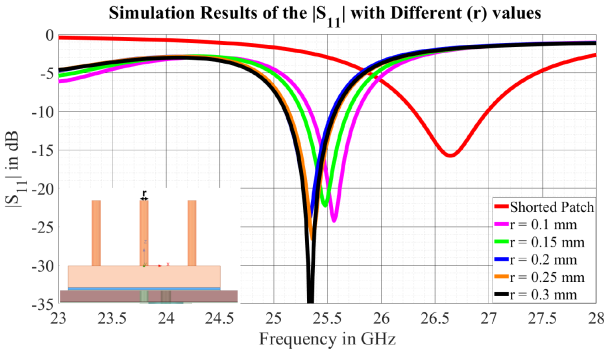

Fig. 9. Frequency dependence of the reflection coefficient for different fin radius(r). ($h_c = h_s = 1.7, h_b = 0.3, d = 1.2mm$)

(x-axis); however, the polarization of the antenna that has fins at d = 1.2mm starts to have polarization on the xz-axis. The polarization behavior stays linear, but the polarization orientation shifts due to vertical surface currents.

E. Radius of Fins

Lastly, the radius of the fins is investigated. This has a minor effect on both the radiation and impedance performance of the antenna. The parametric study on the fin radius and it's S_{11} results can be seen in Fig. 9. The resonance frequency of the antenna shifts to the lower frequencies when one increases the fin radius. This is an expected result as an increase in the fin radius increases the surface current length slightly. The fin radius is used as a fine-tuning element in the design of the heatsink structures shown in the following section.

IV. Heatsink Designs for 24, 26, and 28 GHz Operations and their Numerical Validations

Three different heatsink structures are designed based on the knowledge gained from Section III. The isometric and side view of these antennas can be seen in Fig. 10.

The starting point of this design is to determine the patch and heatsink base size of the antenna at 26 GHz. After selecting these values Antenna B is developed by adding the fin structures. Next, we focused on increasing the resonance frequency of the antenna. To create Antenna C that resonates at 28 GHz, the separation between fin structures is reduced

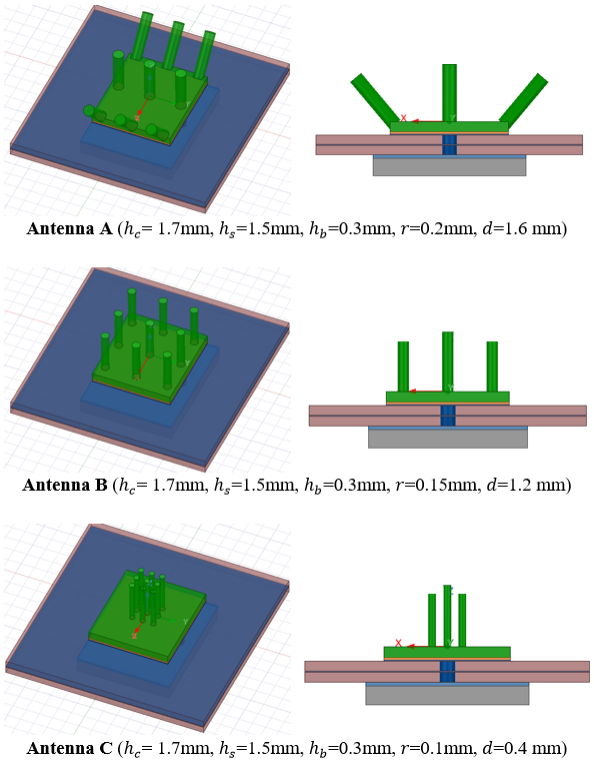

Fig. 10. Isometric and side views of Antenna A (resonates at 24 GHz), Antenna B (resonates at 26 GHz) and Antenna C (resonates at 28 GHz).

and the resonance point is tuned by changing the radius of fins slightly to r = 0.1 mm. Antenna A is created by employing two different mechanisms. In the first mechanism, the distance between fins is increased as much as possible. But, the operating frequency obtained from the d = 1.2 mm case is also not enough to operate at 24 GHz. Design requires more conduction paths for surface currents. The extra path cannot be created by increasing the fin height as explained in Section III; therefore, the fins at the radiating edge are rotated to 40^0 with respect to the z-axis to form an additional current path. This design is tuned to fin radius be r = 0.2mm. The reflection coefficient of antennas can be seen in Fig. 11.

The radiation patterns of Antenna A, B & C can be seen

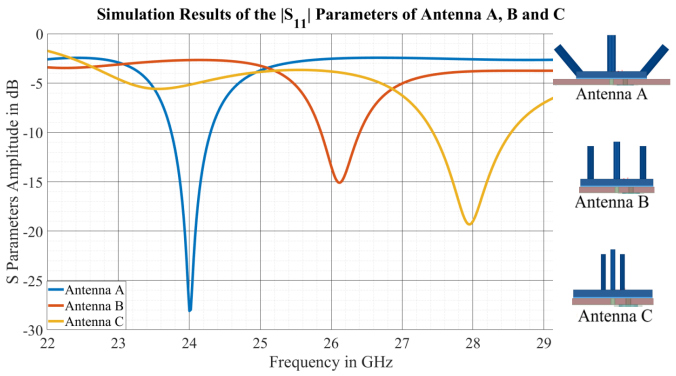

Fig. 11. Reflection Coefficient vs. Frequency of Antenna A, Antenna B and Antenna C.

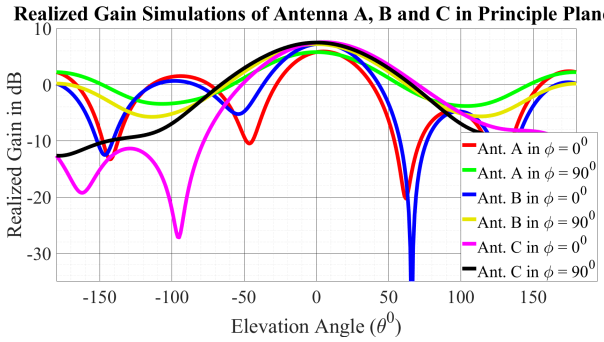

Fig. 12. Radiation pattern simulations of Antenna A (f=24 GHz), Antenna B (f=26 GHz) and Antenna C (f=28 GHz) in $\phi = 0^0$ and $\phi = 90^0$ cut-planes.

TABLE I
ELECTROMAGNETIC PERFORMANCE SUMMARY OF THE SHORTED PATCH AND HEATSINK ANTENNAS

Frequency & Antenna Name	Radiation Efficiency	Total Efficiency	Max. Directivity [dBi]	Max. Gain [dBi]	Max. Realized Gain [dBi]
$f = 24GHz$ Shorted Patch	0.92	0.92	6.91	6.55	6.54
$f = 26GHz$ Shorted Patch	0.94	0.92	7.19	6.92	6.84
$f = 28GHz$ Shorted Patch	0.94	0.9	7.32	7.08	6.99
$f = 24GHz$ Antenna A	0.83	0.8	6.86	6.01	5.9
$f = 26GHz$ Antenna B	0.89	0.85	7.94	7.48	7.25
$f = 28GHz$ Antenna C	0.96	0.95	7.75	7.59	7.54

in Fig. 12. As it can be seen from Fig. 12, all antennas radiate in the broadside direction. The finite size of the ground 7.5mm which corresponds to 0.7λ at 28 GHz results in surface current radiation, so sidelobes occur. Also as antenna A has flared fin structure it excites more surface currents, that yield unwanted radiation at $\theta = 90^0$ and $\theta = -90^0$. The summary of electromagnetic performance of the finned antenna and its comparison with the regular antenna can be seen in Table I.

After investigating the electromagnetic performance of the proposed antennas, we also look at the improvement in the cooling of the chip junction and patch surface temperatures. The computational fluid dynamics based thermal simulations are realized for Antenna A, B & C and maximum temperature values for the chip patch and fins are obtained. The corresponding results are provided in Table II.

Antenna A contributes to cooling more than the other antennas and antenna C has the lowest contribution. This result is expected as antenna A spreads excess heat in a wider area compared to the other ones, and it employs advantages of the forced air cooling more compared to the others. In antenna C, the fin structures are placed so close that the airflow efficiency is lower than the other two antennas and it has less cooling contribution. The cooling performance increases with addition of vias, as these vias provide heat flow to the patch structure.

TABLE II
TEMPERATURES OF HEATSINK ANTENNAS TAKEN FROM CHIP JUNCTION, PATCH SURFACE AND HEATSINK FINS

	Chip Temp.[^0C]	Patch Temp.[^0C]	Heatsink Temp. [^0C]
Conventional Patch	97.52	60.57	none
Shorted Patch in Fig.1	79.84	72.45	none
Antenna A	69.17	62.11	61.74
Antenna B	70.21	63.20	62.87
Antenna C	74.34	67.50	67.24

V. CONCLUSION

An original heatsink-attached patch antenna concept is proposed for dual electro-thermal functionality. Novel pin fin heatsink structures are developed based on the outcomes of the parametric studies on the heatsink dimensions. The proposed antenna can be operated in different mm-wave frequency bands (24, 26, and 28 GHz) by changing the heatsink type. It also contributes to the cooling of the RF chip by 23 to 28 degrees more as compared to conventional patch elements, while keeping similar radiation properties in the operating frequencies. Future work will focus on extensions to arrays.

ACKNOWLEDGMENT

This work was supported by the Microelectronics Department at the Delft University of Technology in the framework of the Synergy Grant. The authors would to like thank Prof. Alexander Yarovoy, from the Delft University of Technology for his valuable comments on the paper.

REFERENCES

[1] W. Hong et al., "The role of millimeter-wave technologies in 5G/6G wireless communications," *IEEE J. Microw.*, vol. 1, no. 1, pp. 101–122, Jan. 2021.
[2] B. Sadhu, X. Gu, and A. Valdes-Garcia, "The more (antennas), the merrier: A survey of silicon-based mm-wave phased arrays using multi-IC scaling," *IEEE Microw. Mag.*, vol. 20, no. 12, pp. 32–50, Dec. 2019.
[3] E. McCune, "Energy efficiency maxima for wireless communications: 5G, IoT, and massive MIMO," in *Proc. IEEE China Int. Capital Corp.*, Austin, TX, USA, May 2017.
[4] Y. Aslan et al., "Thermal-aware synthesis of 5G base station antenna arrays: An overview and a sparsity-based approach," *IEEE Access*, vol. 6, pp. 58 868–58 882, 2018.
[5] B. J. Döring, "Cooling system for a Ka band transmit antenna array," German Aerosp. Center, Cologne, Germany, Tech. Rep. IB554-06/02, Dec. 2005.
[6] Y. Aslan et al., "Passive cooling of mm-wave active integrated 5G base station antennas using CPU heatsinks," in *Proc. 16th EuRAD*, Paris, France, Oct. 2019, pp. 121–124.
[7] Y. Aslan, "Opportunities, progress and challenges in active heatsink antenna arrays for 5G and beyond," in *Proc. 52nd EuMC*, Milan, Italy, Sep. 2022.
[8] L. Covert and J. Lin, "Simulation and measurement of a heatsink antenna: A dual-function structure," *IEEE Trans. Antennas Propag.*, vol. 54, no. 4, pp. 1342–1345, Apr. 2006.
[9] L. Covert, J. Lin, D. Janning, and T. Dalrymple, "5.8 GHz orientation-specific extruded-fin heatsink antennas for 3D RF system integration," *Microw. Opt. Technol. Lett.*, vol. 50, no. 7, pp. 1826–1831, Jul. 2008.
[10] J. Qian, M. Tang, Y.-P. Zhang, and J. Mao, "Heatsink antenna array for millimeter-wave applications," *IEEE Trans. Antennas Propag.*, vol. 68, no. 11, pp. 7664–7669, Nov. 2020.
[11] L. Zhou, M. Tang, Y. P. Zhang and J. Mao, "Electro-thermal design of SIW slot antenna array with fin-shaped heatsink enclosed," *IEEE Trans. Compon. Packag. Manuf. Technol.*, Early Access, 2022.
[12] Two-Resistor Compact Thermal Model Guideline, document JESD-1, JEDEC, Jul. 2008.